IEEE Access
Multidisciplinary ⋮ Rapid Review ⋮ Open Access Journal

Received April 9, 2022, accepted May 2, 2022, date of publication May 9, 2022, date of current version May 17, 2022.

Digital Object Identifier 10.1109/ACCESS.2022.3173806

Location-Based Hybrid Precoding Schemes and QoS-Aware Power Allocation for Radar-Aided UAV–UGV Cooperative Systems

XIANGQIAN XU[1], (Student Member, IEEE), RENMIN ZHANG[1,2], (Member, IEEE), AND YINGJING QIAN[2,1]

[1]College of Information Science and Enginering, Jishou University, Jishou, Hunan 416000, China
[2]Key Laboratory of Intelligent Control Technology for Wuling-Mountain Ecological Agriculture in Hunan Province, Huaihua University, Huaihua, Hunan 418000, China

Corresponding authors: Renmin Zhang (rzhang1981@163.com) and Yingjing Qian (Qyingjing@163.com)

This work was supported in part by the National Natural Science Foundation of China under Grant 62061017, in part by the NSF of Hunan province under Grant 2021JJ30556 and Grant 2022JJ*****(entitled "Research on Localization and Location-Aware Beamforming Technology for Air-Ground Integrated Large-Scale MIMO mmWave Communications"), in part by the Educational Commission of Hunan Province under Grant 19B456, and in part by the Postgraduate Scientific Research Innovation Project of Hunan Province under Grant QL20210244 and Grant CX20201063.

ABSTRACT Unmanned aerial vehicles (UAVs) and unmanned ground vehicles (UGVs) complement each other, promising a variety of benefits for unmanned cooperative systems. When infrastructures for communication are unavailable, such as disaster relief and patrol mission in sparsely populated areas, UGVs can be controlled to go to the esignated areas with the aid of a UAV. Specifically, the UAV hovers over the UGVs, sending commands to the UGVs and obtaining location information from the UGVs. In this paper, we consider integrating millimeter wave communication and UAV–UGV cooperative system. For high mobile unmanned cooperative systems, we develop two joint radar-aided hybrid precoding schemes, which are suitable for a fully connected (FC) hybrid precoding structure and partially connected (PC) hybrid precoding, respectively. Specifically, an effective hybrid precoding scheme is first proposed by using location information to jointly design hybrid precoding and power allocation. Moreover, we also derive the radar parameter estimation problem Cramér-Rao lower bound (CRLB). In order to ensure the minimum quality-of-service (QoS) of UGVs, we propose a QoS-aware power allocation scheme based on the difference-of-two-convex-function (D.C.) programming. Finally, a heuristic hybrid precoding design algorithm, where the analog precoding matrix is usually implemented by low-resolution phase shifters (PSs), is proposed based on antenna dynamic grouping and radar parameter acquisition, with the aim of maximizing the sum-rate of the UAV–UGV cooperative systems. Extensive computer simulation results indicated the validity of the proposed radar-aided location-based hybrid precoding schemes in the UAV–UGV heterogeneous cooperative system.

INDEX TERMS Location-based hybrid precoding, radar-aided UAV–UGV cooperative system, D.C. programming, dynamic antenna grouping.

I. INTRODUCTION

Research on unmanned aerial vehicles (UAVs) and unmanned ground vehicles (UGVs), which aim at meeting diverse emerging application requirements while solving various problems in case of emergency such as communication failure, rescue effort, and post-disaster reconstruction, has recently received extensive attention from both academia and industry [1], [2]. However, due to many indeterminate factors involved in emergency distinctive needs, the separate division of labor between UAV and UGV unavoidably reveals its own insufficiencies [3]. To realize their full potential, UAVs and UGVs can cooperate with each other and complement each other's strengths. Specifically, UAV equipped with a wide-angle camera can be rapidly deployed to a designated area and search for targets in a wide range, but the small payload

The associate editor coordinating the review of this manuscript and approving it for publication was Hasan S. Mir.

and high power consumption limit its capabilities for many applications. On the contrary, UGV with a limited field of view can approach the desired location to accomplish complex missions due to its large payload. However, it is difficult to control from a macroscopic point of view. To address the shortcomings of the above homogeneous system, the UAV–UGV heterogeneous cooperative systems have aroused significant attention [4].

Despite the UAV–UGV cooperative system's potential prospects, substantial research work is needed to actualize the advantages offered by the heterogeneous cooperative system. To satisfy the requirement for exceedingly high data rates and low delays, millimeter wave (mmWave), as one of the most crucial characteristics of 5G mobile networks, is projected to enable ultra-wideband connection with extremely high stability and low delay to improve data rates [5]. Nevertheless, in the mmWave band, the signal suffers from severe propagation loss and and rain-attenuation [6]. Fortunately, more antennas can be deployed in the same size space as compared to conventional communication, because of the shorter wavelength of the mmWave band. Large-scale antenna array can realize highly directional beamforming while compensating for the serious path loss of the mmWave signals by the generated beamforming gain [7]. Consequently, the integration of mmWave wireless communication and the UAV–UGV cooperative system could satisfy the requirement of high data rate transmission in the future. The challenge of combining mmWave massive MIMO systems and UGV–UAV cooperative systems is to design efficient beamforming techniques to reduce the cost and power consumption while weighing system hardware limitations and system performance [8].

Beamforming with multiple data streams, namely precoding, is typically utilized to further enhance the spectral efficiency (SE) of millimeter wave systems. While the principle of precoding is independent of carrier frequency, signal processing in mmWave communication systems is constrained by a number of practical limitations. For instance, fully digital precoding (FDP) is generally used in traditional MIMO systems, which needs one private radio frequency (RF) chain (incorporating expensive digital-to-analog converter) per-antenna elements [9]. Although FDP can guarantee the best performance of mmWave MIMO systems, it is unrealistic from the perspectives of cost and energy consumption in the millimeter-wave band [10]. One approach to solve the aforementioned involves the use of hybrid precoding (HP) solutions. Specifically, a low-dimensional digital precoder is used at the baseband to ensure the performance of the system, and then a few RF chains are used to connect the high dimensional analog precoder (analog domain) controlled by a phase shifter (PS) network to reduce the hardware cost. Two typical HP schemes have been extensively studied for mmWave MIMO systems. Depending on the connection method, the existing HP schemes can be split into fully-connected hybrid precoding (FC-HP) architecture as shown in Fig. 4(a) and partially-connected hybrid precoding (PC-HP) architecture as depicted in Fig. 4(b). For the FC-HP architecture, each RF chain is linked to all antennas via PSs. A low complexity hybrid precoding algorithm on the basis of orthogonal matching pursuit (OMP) was developed by using the sparsity of the millimeter wave channel [11]. However, the behavior of the algorithm is unsatisfactory when the amount of RF chains is fewer than twice of the number of data streams. At the same time, for multiuser mmWave systems, a low-complexity HBF method named phased-ZF (PZF) was presented in [12], which designed an analog precoder by extracting the phase of the conjugate transpose of the cascaded downlink channel and designed a digital precoder through a zero-forcing (ZF) algorithm on the effective channel. The difference with the above problem is that it assumes that the amount of RF chains is the same as the amount of data streams.

However, there is also a problem in FC-HP structures. In order to achieve accurate phase control in RF domain, each RF chain needs to be linked to all antenna elements through PSs. The presence of a significant large number of phase shifters will cause huge power consumption. This has caused a variety of research into the PC-HP structure, so as to offer a compromise between performance and power consumption. Compared with the FC structure, the main difference is that each RF chain of the PC structure can only be attached to a subgroup of antenna elements. The PC-HP architecture was first proposed in [13]. Moreover, a low complexity HP algorithm according to successive interference cancellation (SIC) was developed, and the complexity of this algorithm is only about 10% of the OMP algorithm in [11]. In [14], both FC and PC precoding structures are considered. The hybrid precoding problem is divided into two sub-problems of digital precoding and analog precoding, and the principle of alternating minimization (AltMin) is used to alternately optimize the digital precoder and analog precoder, whereas the algorithm requires the digital and analog precoder to be updated in each iteration, resulting in significant computational complexity. The abovementioned hybrid precoder design usually assumes employment of high-resolution PSs, which requires complex hardware design and has heavy power consumption at mmWave systems. To solve this problem, several works have studied the design of a hybrid precoder with low-resolution PSs for FC-HP architecture and PC-HP architecture [15]–[17].

High-speed mobility (HSM) is another challenging issue that arises in UAV–UGV cooperative systems. Despite the fact that the mmWave has been extensively utilized in static scenes, using it in mobile networks, in which the transmitting/receiving nodes are likely to move, and the channel might have complicated structures, is a significant challenge [18]. To the best of our knowledge, research on precoding design for HSM problems in the mmWave Multi-User Multiple-Input Single-Output (MU-MISO) communication systems is still in its early stages. Furthermore, power allocation and precoding are two approaches for effective cochannel interference management, thereby improving multiuser wireless network performance [19]. However, because joint hybrid precoding and power allocation optimization are frequently

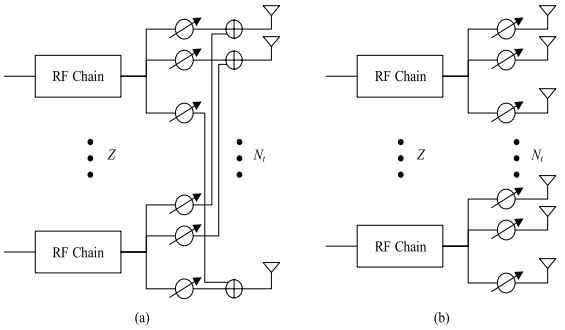

FIGURE 1. Main types of hybrid precoding architectures: (a) fully connected; (b) partially connected (without overlapping).

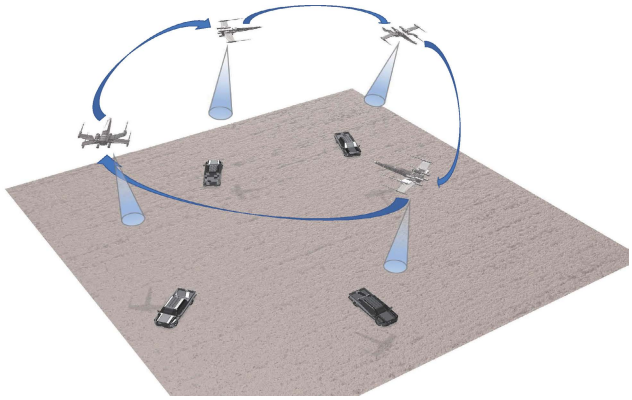

FIGURE 2. The block diagram of the proposed system.

tricky, most known studies dissociate this coupled problem into two separate subproblems. At the same time, the concept of integrated sensing and communication (ISAC) is put forward in the literature [20], which can make full use of spectrum resources by jointly designing a communication system and radar system. Mobile networks are changing from pure communication networks to networks with combined communication and radar abilities. By using traditional radar's tracking, localization and object recognition functions, perception information obtained by radar can be used to assist communication and establish a more stable and effective communication link.

As a result of the aforementioned observations, we propose a location-based hybrid precoding strategy for the mmWave MU-MISO system under radar-aided UAV–UGV cooperative systems. Specifically, two main schemes are developed in this paper. First, based on the motion parameters acquired by radar, an HP scheme with an FC structure is designed, with joint precoding and power allocation to optimize the sum-rate while guaranteeing the quality-of-service (QoS) requirement of each UGV at the same time. In addition, the Cramér-Rao lower bound (CRLB) of the motion parameters estimation problem is deduced. Second, with the aid of a radar system, an HP algorithm with a PC structure is proposed to optimize the sum-rate by dynamically grouping antennas. The major contributions of our work are summarized as follows:

- For the proposed UAV–UGV cooperative system, a radar-aided mmWave communication strategy is presented, in which one UAV can serve several UGVs.
- With the assistance of the radar system, an efficient hybrid precoding scheme is developed for FC structure and PC structure, respectively, to optimize the sum-rate performance of the UAV–UGV cooperative system.
- Taking advantage of radar positioning, firstly, the nonconvex joint hybrid precoding and power allocation optimization problems involved in the FC structure hybrid precoding scheme are modeled as a difference-of-two-convex-function (D.C.) programming problem, so as to optimize the sum-rate while meeting the minimum QoS requirements.
- For the purpose of reducing system power consumption, we further present a novel heuristic hybrid precoding algorithm based on a dynamic antenna grouping for PC architecture. Due to the use of motion parameters obtained by radar, the proposed algorithm complexity is further reduced.
- In terms of positioning error, the positioning accuracy is evaluated using the upper bound of positioning error

The remainder of this paper is laid out as follows: In Section II, we present the system model of the proposed radar-aided UAV–UGV cooperative system. Section III describes the signal processing of the radar system. In Section IV and Section V, the detailed description of our proposed radar-aided FC-based and PC-based hybrid precoding scheme is given, respectively. Section VI provides the extensive simulations results. A detailed conclusion of our paper is given in Section VII.

Notation: Throughout this paper, we will use the following notation: Uppercase boldface letters represent matrices and lowercase boldface letters denote vectors. $\boldsymbol{I}_N$ represents the $N \times N$ identity matrix. $\|\boldsymbol{A}\|$ represents the L2-norm of $\boldsymbol{A}$. $\|\boldsymbol{a}\|_p$ stands for the p-norm of $\boldsymbol{a}$. $|\boldsymbol{A}|$ denotes the determinant of $\boldsymbol{A}$, while $|A|$ represents the cardinality of set A. $\hat{\boldsymbol{a}}$ denotes the estimator of $\boldsymbol{a}$, and $\mathrm{Re}\{\boldsymbol{a}\}$ represents the real part of $\boldsymbol{a}$, in which $\hat{\boldsymbol{a}}$ and $\boldsymbol{a}$ may be a scalar, vector, or matrix. $\boldsymbol{A}^T$ represents the transpose of $\boldsymbol{A}$, and $\boldsymbol{A}^H$ denotes the conjugate transpose of $\boldsymbol{A}$. Lastly, $\nabla f(\boldsymbol{x})$ denotes the gradient of function $f(\boldsymbol{a})$. The inner product of $\boldsymbol{a}$ and $\boldsymbol{b}$ is represented as $\langle \boldsymbol{a}, \boldsymbol{b} \rangle = \boldsymbol{a}^T \boldsymbol{b}$.

II. SYSTEM MODEL

In this section, we describe a radar-aided hybrid precoding system and channel model that takes user mobility and large-scale fading into account.

A. SYSTEM OVERVIEW

The schematic diagram is illustrated in Fig. 2, in which a UAV loaded with a mmWave base station (BS) and monostatic radar hovers over UGVs. Specifically, for the communication function of the UAV, the UAV-BS has N_t transmit antennas and Z RF chains, which send Z data streams to Z UGVs with a single antenna for receiving communication

information, respectively. In addition, the number of RF chains is normally much smaller than the amount of antennas in the actual system, i.e., $Z \ll N_t$. In order to enable the radar sensing capability of the UAV, the monostatic radar loaded on the UAV is set up separately with N_r receiving antennas in addition to sharing N_t transmitting antennas of the UAV-BS [21]. Further, in the proposed system, due to the limitation of the RF chain, the maximum number of transmission streams is limited to Z. We assume that each scheduled UGV only allocates one data stream for transmission. $s \in \mathbb{R}^Z$ represents the vector of transmitted symbols.

To establish connectivity, the UAV first periodically scans the space until it is recognized by UGVs. In addition, we suppose a UAV communicates with Z UGVs and simultaneously locates them with radar. The z-th UGV's and UAV's horizontal positions is defined as $p_z^G = \left[x_z^G, y_z^G\right]$ and $p^U = \left[x^U, y^U\right]$, respectively.

Consider a multiuser mmWave downlink MISO system where a UAV-BS with N_t antennas communicates to Z single-antenna UGVs. Each antenna of the UAV-BS is marked separately as $1, 2, \ldots, N_t$, and $T = \{1, 2, \ldots, N_t\}$. Each of the Z UGVs is labeled, respectively, as $1, 2, \ldots, Z$, and $U = \{1, 2, \ldots, Z\}$.

B. LARGE-SCALE FADING

The z-th UGV's horizontal distance from the UAV is defined as

$$G_z = \sqrt{(x^U - x_z^G)^2 + (y^U - y_z^G)^2}. \tag{1}$$

We utilize a Low Altitude Platform (LAP) that was established in [22]. The air-to-ground (ATG) path loss between the z-th UGV and the UAV could be expressed in dB as

$$\mathcal{L}_z^{\mathrm{dB}} = \frac{\eta_{\mathrm{LoS}} - \eta_{\mathrm{NLoS}}}{1 + a\exp(-b\left[\arctan(\frac{h}{G_z}) - a\right])} + 20\log(d_z) + C_{LAP}, \tag{2}$$

where

$$d_z^2 = h^2 + G_z^2, \tag{3}$$

$$C_{\mathrm{LAP}} = 20\log f + 20\log(4\pi/c) + \eta_{\mathrm{NLoS}}, \tag{4}$$

with a and b representing the Sigmoid-curve (S-curve) parameters, and η_{LoS} and η_{NLoS} separately denote the excessive path loss in the conditions of line-of-sight (LoS) and non-line-of-sight (NLoS). h is the height of the UAV, f is the system frequency, and d_z is the practical distance between the z-th UGV and UAV. c is the velocity of light.

C. COMMUNICATION CHANNEL MODEL

We consider a high path-loss propagation setting with a finite amount of scatters, assuming that each scatter contributes just one propagation path. For this reason, we utilize Saleh-Valenzuela (SV) channel model, as illustrated in [12]. Eventually, the z-th user's channel vector $\boldsymbol{H}_z$ can be formulated as

$$\boldsymbol{H}_z = \sqrt{\frac{N_t}{L_z}} \sum_{l=1}^{L_z} \alpha_{z,l} \cdot \boldsymbol{a}_t^H\left(\theta_{z,l}\right) \tag{5}$$

where L_z is the amount of all propagation paths and $\alpha_{z,l}$ is the complex gain of the l-th scattering cluster, whereas $\theta_{z,l}$ is its angle of departure (AOD). Eventually, the vector $\boldsymbol{a}_t(\theta)$ denotes the normalized transmit array response vector. Although the algorithms and results deduced in the rest of this paper are effective in any antenna array configuration, in this paper, we assume that an M-element uniform linear array (ULA) is utilized at UAV-BS. The transmit array response vector $\boldsymbol{a}_t(\theta)$ can be defined as

$$\boldsymbol{a}_t(\theta) = \frac{1}{\sqrt{M}}\left[1, e^{jkd\sin(\theta)}, \ldots, e^{j(M-1)kd\sin(\theta)}\right]^T \tag{6}$$

where $k = \frac{2\pi}{\lambda}$ represents the wavenumber of the signal, and d denotes the inter-antenna space.

D. HYBRID PRECODING

In our proposed hybrid precoding system, let $\boldsymbol{\mu} := (\mu_1, \mu_2, \ldots, \mu_z)^T$ represent the transmitted power vector, each component μ_z of which denotes the transmitted power of z-th UGV, σ_z^2 represents the noise power. Observing the comparable expressions in [12], we are committed to the design of digital and analog precoders. Firstly, the transmitted symbols of Z UGV are precoded by a digital precoding matrix $\boldsymbol{F} = [\boldsymbol{f}_1, \boldsymbol{f}_2, \ldots, \boldsymbol{f}_Z] \in \mathbb{R}^{Z\times Z}$. Then, there is an analog precoding matrix $V = [\boldsymbol{v}_1, \boldsymbol{v}_2, \ldots, \boldsymbol{v}_Z] \in \mathbb{R}^{N_t\times Z}$ with $\boldsymbol{v}_k = [v_{k,1}, v_{k,2}, \ldots, v_{k,N_t}]^T$ in the RF domain. It is worth noting that the amplitude and phase adjustment is workable for the digital precoder F; however, due to hardware constraints, phase modification can only be performed on the analog precoder V. Consequently, each element of V is normalized to meet the $\left|v_{i,j}\right| = \frac{1}{\sqrt{N_t}}$, where $\left|v_{i,j}\right|$ represents the magnitude of the (i,j)th entry of V. Moreover, analog precoding is performed through the use of low-resolution PS in practical implementation, each with quantized phases controlled by B bits. Each entry of the analog precoder can be represented as $v_{i,j} \in \left\{\frac{1}{\sqrt{N_t}} e^{-j\frac{2\pi n}{2^B}} \middle| n = 0, 1, \ldots, 2^B - 1\right\}$. V and F are related through the power constraints,i.e., $\|\boldsymbol{VF}\|_F^2 = Z$.

Let $y = [y_1, y_2, \ldots, y_Z]^T$ represent the received signal of Z UGVs, and the received signal vector of the z-th UGV can be defined as

$$y_z = H_z \sum_{z=1}^{Z} \boldsymbol{V} f_z s_z + n_z, \forall z, \tag{7}$$

where s_z, $z = 1, \ldots, Z$, represents the transmit symbol of the z-th UGV. All transmit symbols are individual across the UGVs, $\mathbb{E}[\boldsymbol{ss}^H] = \frac{P}{Z}\boldsymbol{I}_Z$ where P denotes total transmit power of the UAV-BS. H_z, $z = 1, \ldots, Z$, denotes the channel between the the z-th UGV and UAV. n_z stands for the complex Gaussian noise (i.i.d.), which is presumed to be circularly symmetric Gaussian with variance σ_z^2.

To simplify the subsequent symbolic representation, we denoted by g_z^H the effective analog precoding gain of the z-th UGV,i.e.,

$$\boldsymbol{g}_z^H = \boldsymbol{H}_z \boldsymbol{V} \tag{8}$$

Furthermore, the signal-to-interference-plus-noise ratio (SINR) of the z-th UGV can be defined as

$$SINR_z = \frac{\mu_z |\boldsymbol{g}_z^H \boldsymbol{f}_z|^2}{\sum_{i=1, i\neq z}^{Z} \mu_i |\boldsymbol{g}_z^H \boldsymbol{f}_i|^2 + \sigma_{n,z}^2} \tag{9}$$

The resulting achievable rate of z-th UGV is represented as

$$R_z = \log_2 \left(1 + \frac{\mu_z |\boldsymbol{g}_z^H \boldsymbol{f}_z|^2}{\sum_{i=1, i\neq z}^{Z} \mu_i |\boldsymbol{g}_z^H \boldsymbol{f}_i|^2 + \sigma_{n,z}^2} \right). \tag{10}$$

Finally, the sum-rate of the proposed UAV–UGV cooperative system can be calculated as

$$R = \sum_{z=1}^{Z} \log_2(1 + SINR_z) \tag{11}$$

III. SIGNAL PRECODING AND DECODING OF THE RADAR SYSTEM

In this section, a radar system for the auxiliary mmWave communication system to acquire angle parameters is elaborated.

A. RADAR PRECODING SYSTEM

In order to determine the status of the UGV, the monostatic radar transmits a multibeam signal $\boldsymbol{s}(t) \in \mathbb{C}^Z$, i.e.,

$$\boldsymbol{s}(t) = [s_1(t), \cdots, s_Z(t)]^T, \tag{12}$$

where $s_z(t)$ denotes the signal pointing to the z-th UGV.

We suppose the radar signal $s_z(t)$ is emitted by using an uniform steering vector $\boldsymbol{a}(\phi_z)$, which is formulated by

$$\boldsymbol{a}(\phi_z) = \sqrt{\frac{1}{N_t}} [1, e^{j\pi \sin\phi_z}, \cdots, e^{j(N_t-1)\pi \sin\phi_z}], \tag{13}$$

where ϕ_z is the angle of the z-th UGV in the targeted direction of the UAV. The receive uniform steering vector can then be represented in the same manner.

The emitted signal is reflected back by Z UGV. Then, the roundtrip echo is captured by the sensing detector. From the UAV perspective, the channel for z-th UGV and UAV will be modeled as

$$\boldsymbol{H}(t, \tau) = \beta_z G_a \boldsymbol{b}(\theta_z) \boldsymbol{a}^H(\theta_z) \delta(\tau - \gamma_z) e^{j2\pi\omega_z t}, \tag{14}$$

where $G_a = \sqrt{N_t N_r}$ denotes the antenna array gain. $\boldsymbol{b}(\theta_z)$ represents the received uniform steering vector, meeting $\boldsymbol{b}(\theta_z) = \boldsymbol{a}(\theta_z)$, because θ_z is the practical angle of the UAV designated to the z-th UGV. Additionally, the parameters γ_z, ω_z, and β_z represent the time delay, Doppler spread, and reflection damping coefficient related to z-th UGV, respectively.

Eventually, the received echo $\boldsymbol{r}(t) \in \mathbb{C}^{N_r}$ is defined as

$$\boldsymbol{r}(t) = \sum_{z=1}^{Z} \beta_z G_a \boldsymbol{b}(\theta_z) \boldsymbol{a}^H(\theta_z) \boldsymbol{P} \boldsymbol{s}(t - \gamma_z) e^{j2\pi\omega_z t} + \tilde{\boldsymbol{n}}(t), \tag{15}$$

where $\tilde{\boldsymbol{n}}(t)$ represents the complex Gaussian noise vector, and $\boldsymbol{P}$ is a precoding matrix whose z-th column is represented as $\boldsymbol{P}_z = \sqrt{p_z}\boldsymbol{a}(\phi_z)$.

Considering the characteristics of the large mmWave MIMO system, the array response vectors $\boldsymbol{a}(\theta)$ for various angles θ are asymptotically orthogonal [23], i.e.,

$$\boldsymbol{a}^H(\theta_i)\boldsymbol{a}(\theta_j) \approx 0, \quad \text{for} \quad i \neq j. \tag{16}$$

Benefiting from this, the UAV can identify the echoes reflected back from different UGVs, i.e., $\boldsymbol{r}(t) = [r_1(t), \cdots, r_Z(t)]^H$. More specifically, after receiving all the reflected signals from the UGVs, the UAV will perform matched filtering with a group of emitted signals, and finally, the received echo from the z-th UGV can be denoted as:

$$\begin{aligned} \tilde{\boldsymbol{r}}_z(\gamma, \omega) &= \int_0^{\delta T} r_z(t) s_z^*(t - \gamma) e^{-j2\pi\omega t} \mathrm{d}t \\ &= \int_0^{\delta T} \beta_z G_a \boldsymbol{b}(\theta_z) \boldsymbol{a}^H(\theta_z) \\ &\quad \cdot \boldsymbol{P} s_z(t - \gamma_z) s_z^*(t - \gamma) e^{j2\pi(\omega - \omega_z)t} \mathrm{d}t + \tilde{\boldsymbol{n}}_z, \end{aligned} \tag{17}$$

where δT represents the frame duration. γ and ω represent the time delay and Doppler shift, respectively. Further, it is worth noting that after matched filtering the estimates of the signaling delay and Doppler shift associated with the corresponding UGVs can be derived, denoted as $\hat{\gamma}_z$ and $\hat{\omega}_z$, respectively. Moreover, the filtered complex Gaussian noise vector can be expressed as

$$\tilde{\boldsymbol{n}}_z = \int_0^{\delta T} \tilde{\boldsymbol{n}}(t) s_z^*(t - \gamma) e^{-j2\pi\omega t} \mathrm{d}t. \tag{18}$$

When the corresponding delay and Doppler shift are estimated, a sample of the echo signal from the z-th UGV can be derived by

$$\boldsymbol{r}_z = \sqrt{p_z} G_t G_a \beta_z \boldsymbol{b}(\theta_z) \boldsymbol{a}^H(\theta_z) \boldsymbol{a}(\phi_z) + \tilde{\boldsymbol{n}}_z, \tag{19}$$

where p_z represents the allocated transmit power to the z-th UGV, and G_t denotes the signal-to-noise ratio (SNR) gain derived after matched filtering, which is the same as the energy of the emitted signal.

B. CRLB OF THE TIME DELAY IN SIGNAL PROPAGATION

We suppose that the radar-equipped UAV emits signals to search for UGVs. Once detected, the signals return within a short time period.

The discrete signal N samples received are denoted by

$$\hat{s}_\ell = s(\ell T_\ell - \tau_\ell) + n_\ell, \quad \text{for} \quad \ell = 0, 1, \cdots, N-1, \tag{20}$$

where T_ℓ represents the frame duration of the ℓ-th and $(\ell + 1)$-th discrete samples. The emitted signal

$s(\ell T_\ell - \tau_\ell)$ suffers a time delay τ_ℓ before it is received by the UGV. n_ℓ denotes the complex Gaussian noise.

For a given received signal $\hat{\boldsymbol{s}} = \{\hat{s}_\ell\}_{\ell=0,1,\cdots,N-1}$, its posteriori probability is defined by

$$p(\boldsymbol{\tau}|\hat{\boldsymbol{s}}) = \frac{p(\hat{\boldsymbol{s}}|\boldsymbol{\tau})p(\boldsymbol{\tau})}{p(\hat{\boldsymbol{s}})}. \tag{21}$$

The maximum a posteriori (MAP) estimation expressed as

$$\hat{\boldsymbol{\tau}}(\hat{\boldsymbol{s}}) = \arg\max_{\boldsymbol{\tau}} p(\boldsymbol{\tau}|\hat{\boldsymbol{s}}) = \arg\max_{\boldsymbol{\tau}} p(\hat{\boldsymbol{s}}|\boldsymbol{\tau})p(\boldsymbol{\tau}). \tag{22}$$

For the sake of simplification, we consider using logarithmic probability for maximum likelihood (ML) estimation:

$$\hat{\boldsymbol{\tau}}(\hat{\boldsymbol{s}}) = \arg\max_{\boldsymbol{\tau}} \quad \ln p(\hat{\boldsymbol{s}}|\boldsymbol{\tau}), \tag{23}$$

where $p(\hat{\boldsymbol{s}}|\boldsymbol{\tau})$ represents the multiple Gaussian distribution as follows

$$p(\hat{\boldsymbol{s}}|\boldsymbol{\tau}) = (\pi\sigma^2)^{(-N)} e^{-1/\sigma^2 \sum_{\ell=0}^{N} |\hat{s}_l - s(\ell T_\ell - \tau_\ell)|^2}. \tag{24}$$

By analyzing Equation (24), the ML estimation problem (23) can be equated to the problem of minimizing the Euclid's distance between the emitted signal and the echo signal as follows:

$$\begin{aligned}\hat{\boldsymbol{\tau}}(\hat{\boldsymbol{s}}) &= \arg\min_{\boldsymbol{\tau}} \sum_{\ell=0}^{N-1} |\hat{s}_\ell - s(\ell T_\ell - \tau_\ell)|^2, \\ &= \arg\min_{\boldsymbol{\tau}} \sum_{\ell=0}^{N-1} \Big[|\hat{s}_\ell|^2 + |s(\ell T_\ell - \tau_\ell)|^2 \qquad (25) \\ &\qquad -2\mathrm{Re}\{\hat{s}_\ell s(\ell T_\ell - \tau_\ell)^H\} \Big]. \qquad (26)\end{aligned}$$

Since $|s(\ell T_\ell - \tau_\ell)|^2$ denotes the constant associated with $\boldsymbol{\tau}$, the estimation of $\hat{\boldsymbol{\tau}}$ is represented by

$$\hat{\boldsymbol{\tau}}(\hat{\boldsymbol{s}}) = \arg\max_{\boldsymbol{\tau}} \left| \sum_{\ell=0}^{N-1} \hat{s}_\ell s(\ell T_\ell - \tau_\ell)^H \right|. \tag{27}$$

In the actual situation, the higher the signal sampling frequency, the smaller the variation of the time delay. Therefore, the mean value of N samples can be used to approximate the time delay, i.e., $\hat{\tau}_{\text{avg}} = \frac{1}{N}\sum_{\ell=0}^{N-1} \tau_\ell$.

Then, we examine the CRLB of the time delay with complex Gaussian noise. Through the observation of $\hat{\boldsymbol{s}}$, the CRLB of the time delay estimation can be expressed as [25]

$$\mathrm{VAR}(\hat{\tau}_{\text{avg}}) \geq \frac{\sigma^2}{2\sum_{\ell=0}^{N-1} |\frac{d}{d\tau_\ell} s(\ell T_\ell - \tau_\ell)|}. \tag{28}$$

According to the analysis of Equation (28), the CRLB is affected by noise power. The positioning accuracy can be enhanced by improving the SNR. Observing Equation (2), the function related to the distance between the UAV and UGV can be used to measure the positioning accuracy.

IV. RADAR-AIDED FC-BASED HYBRID PRECODING SCHEME

In this section, first, we discuss the FC-based hybrid precoding design for the radar-aided UAV–UGV cooperative systems. Then, the sum rate of the UAV–UGV cooperative system is jointly optimized by D.C. programming, combined with FC-based hybrid precoding and power allocation.

A. OPTIMAL ANGLE ESTIMATION

Based on the received signal in Equation (19), the monostatic radar carried on a UAV has the ability to infer the angle parameters and reflection coefficients [26]. The reflection damping coefficient β_z is given by

$$\beta_z = \frac{\zeta}{d_z} \tag{29}$$

where ζ denotes the radar cross section (RCS) [27], and d_z represents the roundtrip distance from the z-th UGV. The delay of the radar echo γ_z can be calculated by

$$\gamma_z = \frac{d_z}{c} \tag{30}$$

where c is the signal propagation speed. Further, the estimate of β_z can be easily derived as

$$\hat{\beta}_z = \frac{\zeta}{c\hat{\gamma}_z} \tag{31}$$

Substituting Equation (31) into Equation (19) and using standard mathematical manipulation, we obtain

$$\boldsymbol{r}_z = \hat{\beta}_z G_a \sqrt{p_z} \begin{bmatrix} 1 \\ e^{j\pi \sin\theta_z} \\ \cdots \\ e^{j\pi(N_r-1)\sin\theta_z} \end{bmatrix} \cdot \sum_{z=1}^{N_t} e^{j\pi(i-1)(sin\bar{\theta}_z - sin\theta_z)} + n_z \tag{32}$$

where $\bar{\theta}_z$ is the predicted angle. Then, our goal is to maximize the likelihood function $p(\boldsymbol{r}_z|\theta_z)$. To determine the number of the transmit antennas, we can use N_t discrete angles to represent the possible values of θ_z, expressed as $\Xi = \left\{ \frac{\pi}{N_t}, \frac{2\pi}{N_t}, \cdots, \pi \right\}$. To simplify the estimation process, of maximum likelihood function $p(\boldsymbol{r}_z|\theta_z)$ by selecting the values approximate to the predicted angle $\bar{\theta}_z$ in the set Ξ.

Eventually, from the viewpoint of ML estimation, the likelihood maximization of the likelihood function can be calculated as follows:

$$\hat{\theta}_z = \arg\max_{\theta_z \in \Xi} p(\boldsymbol{r}_z|\theta_z) \tag{33}$$

By solving the above equation, we can obtain the optimal estimated angle $\hat{\theta}_z$, for $z = 1, .., Z$. Furthermore, these optimal angles will be used to construct the analog precoding matrix in mmWave MIMO systems with FC-HP structures.

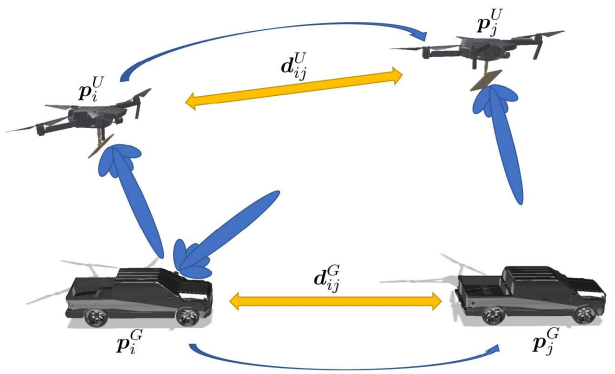

FIGURE 3. The measurement model of the proposed system.

B. ANALOG PRECODER DESIGN

The measurement scenario is shown in Fig. 3. At the i-th moment, we use $\boldsymbol{p}_i^U \in \mathbb{R}^2$ with altitude h represent the position of UAV and $\boldsymbol{p}_i^G \in \mathbb{R}^2$ to denote the positon of UGV. Further, it is assumed that the height of the UAV is constant during the flight. The linear motion is assumed over the estimation period for both UAV and UGV [28]. From location $\boldsymbol{p}_i^U$, the UAV moves in a linear trajectory with known velocity $\boldsymbol{v}_i^U \in \mathbb{R}^2$. Then, the returned pilot is received at another location $\boldsymbol{p}_j^U$. According to the Nyquist sampling theorem, we assume that the channel is sampled by the pilot at a rate not less than twice the maximum Doppler shift, i.e., $\frac{1}{T_p} \geq 2f_D$, where T_p denotes the time spacing between two adjacent pilots, and f_D is the maximum Doppler frequency. Using this assumption, the signal information can be fully transmitted between the UAV and UGV. The propagation speed of beam is a constant c.

We denote the distance between a UGV and a UAV by d_i^{ug} at the i-th instant, i.e.,

$$d_i^{\mathrm{ug}} = \|\boldsymbol{p}_i^U - \boldsymbol{p}_i^G\|. \tag{34}$$

The ideal roundtrip distance traveled is given by

$$r_i = d_i^{\mathrm{ug}} + \|\boldsymbol{p}_j^U - \boldsymbol{p}_i^G\|. \tag{35}$$

Assuming the UAV is moving in a linear trajectory, the position of the UAV at the j-th instant is represented by

$$\boldsymbol{p}_j^U = \boldsymbol{p}_i^U + \frac{\|\boldsymbol{p}_j^U - \boldsymbol{p}_i^G\|}{c}\boldsymbol{v}_i^U, \tag{36}$$

where $\boldsymbol{v}_i^U = \dot{\boldsymbol{p}}_i^U$ is the unknown linear velocity of the UGV.

When the echo signal is received, the UGV's position at the j-th instant is

$$\boldsymbol{p}_j^G = \boldsymbol{p}_i^G + \frac{r_i}{c}\boldsymbol{v}_i^G. \tag{37}$$

Once the location parameter at the i-th moment $\boldsymbol{p}$ is acquired, the predicted actual angle $\theta_{z,i}$ of the z-th UGV at i-th moment with respect to UAV is denoted as

$$\tan\bar{\theta}_{z,i} = \frac{h}{\|\boldsymbol{p}_{z,i}^U - \boldsymbol{p}_{z,i}^G\|}. \tag{38}$$

We assume that the speed of the UGV remains constant for a certain time, and the predicted position at the j-th moment is represented as

$$\tilde{\boldsymbol{p}}_{z,j} = \boldsymbol{p}_{z,i}^G + \Delta T \boldsymbol{v}_{z,i}^G, \tag{39}$$

where $\boldsymbol{v}_{z,i}^G$ is the speed of the z-th UGV at the i-th moment.

According to the ML estimation theory shown in Equation (33), the optimal angle $\hat{\theta}_z$ can be found by maximizing the likelihood function $p(\boldsymbol{r}_i|\theta_z)$.

Based on the channel model adopted in [12], the analog precoding matrix of the FC-HP structure can be denoted by

$$\boldsymbol{V} = [\boldsymbol{v}_1, \boldsymbol{v}_2, \cdots, \boldsymbol{v}_Z], \tag{40}$$

where each element is designed as

$$\boldsymbol{v}_z = [1, e^{j\kappa d \sin\hat{\theta}_z}, \cdots, e^{j(N_t-1)\kappa d \sin\hat{\theta}_z}], \tag{41}$$

C. DIGITAL PRECODER DESIGN

In the Section IV-B, the analog precoder can be obtained by taking advantage of the positioning information acquired by the radar system. Next, in order to eliminate interference between different UGVs, a digital precoder can be constructed. In simple terms, the digital precoding matrix is designed into the pseudo inverse of the effective channel using the block zero-forcing (BZF) algorithm [12]:

$$\boldsymbol{F}^{\mathrm{BZF}} = \boldsymbol{\mathcal{G}}^H(\boldsymbol{\mathcal{G}}\boldsymbol{\mathcal{G}}^H)^{-1}, \tag{42}$$

where $\boldsymbol{\mathcal{G}}$ represents the effective channel, i.e., $\boldsymbol{\mathcal{G}} = [\boldsymbol{g}_1, \boldsymbol{g}_2, \cdots, \boldsymbol{g}_Z]^H$.

In order to meet the standardization constraint, i.e., $\|\boldsymbol{V} \cdot \boldsymbol{f}_z\| = 1$, we perform power standardization for each $\boldsymbol{f}_z$ originating from $\boldsymbol{F} = [\boldsymbol{f'}_1, \boldsymbol{f'}_2, \cdots, \boldsymbol{f'}_Z]$, each element is defined as

$$\boldsymbol{f'}_z = \frac{\boldsymbol{f}_z}{\|\boldsymbol{V} \cdot \boldsymbol{f}_z\|}. \tag{43}$$

D. QoS-AWARE POWER ALLOCATION SCHEME

In this section, we propose a QoS-aware power allocation scheme using the D.C. programming method for given precoders and UGV locations.

The large path loss in the channel between the UAV and the UGV results in the dominance of large scale fading. By estimating and predicting the UGV position parameters, we can derive the received power as follows

$$p_z^{\mathrm{dB}} = \mu_z^{\mathrm{dB}} - \mathcal{L}_z^{\mathrm{dB}}, \tag{44}$$

where $\mathcal{L}_z^{\mathrm{dB}}$ is the path loss calculated using Equation (2).

Taking into account the large scale fading between the UAV and the UGV caused by the distance, finally, according to Equation (10), the achievable rate of the z-th UGV is reformulated as

$$R_z = \log_2\left(1 + \frac{\frac{\mu_z}{\mathcal{L}_z} \cdot |\boldsymbol{g}_z^H \boldsymbol{f}_z|^2}{\sum_{i=1, i\neq z}^{Z} \frac{\mu_i}{\mathcal{L}_i} \cdot |\boldsymbol{g}_z^H \boldsymbol{f}_i|^2 + \sigma_{n,z}^2}\right), \tag{45}$$

where $\mu_z = 10^{\frac{\mu_z^{\mathrm{dB}}}{10}}$, $p_z = 10^{\frac{p_z^{\mathrm{dB}}}{10}}$, and $\mathcal{L}_z = 10^{\frac{\mathcal{L}_z^{\mathrm{dB}}}{10}}$.

Due to the need to safeguard the QoS requirements of UGVs, the sum-rate optimization problem is defined as:

$$\begin{aligned} \underset{\boldsymbol{\mu}}{\text{maximize}} \quad & \sum_{z=1}^{Z} R_z(\boldsymbol{\mu}) \\ \text{subject to} \quad & C_1 : \sum_{z=1}^{Z} \mu_z \le P; \\ & C_2 : R_z(\boldsymbol{\mu}) \ge \lambda_z, z = 1, \ldots, Z. \end{aligned} \tag{46}$$

where C_1 represents the power constraint limited by P, and C_2 guarantees the each UGV's QoS at the lowest required data rate λ.

According to the steps in [29], the sum-rate maximization problem will be remodeled as the D.C. programming problem shown below:

$$\underset{\boldsymbol{\mu}}{\text{maximize}} \quad f(\boldsymbol{\mu}) - g(\boldsymbol{\mu}) \tag{47}$$

where

$$f(\boldsymbol{\mu}) = \sum_{z=1}^{Z} \log_2 \left(\sum_{i=1}^{Z} \frac{\mu_i}{\mathcal{L}_i} \cdot |\boldsymbol{g}_i^H \boldsymbol{f}_i|^2 + \sigma_{n,z}^2 \right),$$

$$g(\boldsymbol{\mu}) = \sum_{z=1}^{Z} \log_2 \left(\sum_{i=1, i\neq z}^{Z} \frac{\mu_i}{\mathcal{L}_i} \cdot |\boldsymbol{g}_z^H \boldsymbol{f}_i|^2 + \sigma_{n,z}^2 \right).$$

From observations based on Equation (47), $f(\boldsymbol{\mu})$ and $g(\boldsymbol{\mu})$ are both concave with respect to $\boldsymbol{\mu}$, i.e., Equation (47) denotes the D.C. functions. For $z = 1,2,\ldots,Z$, we assume that $\boldsymbol{e}_z \in R^Z$ is $\boldsymbol{e}_z(z) = 0$, $z = 1,2,\ldots,Z$ and $\boldsymbol{e}_z(i) = \frac{1}{\ln 2 \cdot \mathcal{L}_i} \cdot |\boldsymbol{g}_z^H \boldsymbol{f}_i|^2$, $i \neq z$. Finally, $\nabla g(\boldsymbol{\mu})$ represents the gradient of $g(\boldsymbol{\mu})$, as shown below

$$\nabla g(\boldsymbol{\mu}) = \sum_{z=1}^{Z} \frac{1}{\sigma_{n,z}^2 + \sum_{i=1, i\neq z}^{Z} \frac{\mu_i}{\mathcal{L}_i} \cdot |\boldsymbol{g}_z^H \boldsymbol{f}_i|^2} \cdot \boldsymbol{e}_z. \tag{48}$$

Selecting a feasible solution $\boldsymbol{\mu}^{(0)}$, the optimal solution $\boldsymbol{\mu}^{(n+1)}$ is generated as the optimum solution of the problem (47) in the n-th iteration:

$$\max_{\boldsymbol{\mu}} f(\boldsymbol{\mu}) - g(\boldsymbol{\mu}^n) - \langle \nabla g(\boldsymbol{\mu}^{(n)}), \boldsymbol{\mu} - \boldsymbol{\mu}^{(n)} \rangle, \tag{49}$$

The above problems can be easily solved by CVX. The running complexity of Formula (49) is $\mathcal{O}(Z^3)$ in each iterative process, as mentioned in [29].

Because $g(\boldsymbol{\mu})$ is a concave function, its gradient $\nabla g(\boldsymbol{\mu})$ is also a super gradient [30], so it has the following properties:

$$\begin{aligned} & f(\boldsymbol{\mu}^{(n+1)}) - g(\boldsymbol{\mu}^{(n+1)}) \\ & \ge f(\boldsymbol{\mu}^{(n+1)}) - \left[g(\boldsymbol{\mu}^{(n)}) + \langle \nabla g(\boldsymbol{\mu}^{(n)}), \boldsymbol{\mu}^{(n+1)} - \boldsymbol{\mu}^{(n)} \rangle \right]. \end{aligned} \tag{50}$$

Furthermore, since $\boldsymbol{\mu}^{(n+1)}$ is also a solution of Equation (49), it meets the following equation

$$f(\boldsymbol{\mu}^{(n+1)}) - g(\boldsymbol{\mu}^{(n)}) - \langle \nabla g(\boldsymbol{\mu}^{(n)}), \boldsymbol{\mu}^{(n+1)} - \boldsymbol{\mu}^{(n)} \rangle, \tag{51a}$$

$$\ge f(\boldsymbol{\mu}^{(n)}) - g(\boldsymbol{\mu}^{(n)}) - \langle \nabla g(\boldsymbol{\mu}^{(n)}), \boldsymbol{\mu}^{(n+1)} - \boldsymbol{\mu}^{(n)} \rangle, \tag{51b}$$

$$\ge f(\boldsymbol{\mu}^{(n)}) - g(\boldsymbol{\mu}^{(n)}). \tag{51c}$$

Consequently, it is easy to see the conclusion that the $(n+1)$-th solution is invariably superior to the (n)-th solution. The criterion for the termination of the iteration is when $|f(\boldsymbol{\mu}^{(n+1)}) - g(\boldsymbol{\mu}^{(n+1)}) - (f(\boldsymbol{\mu}^{(n)}) - g(\boldsymbol{\mu}^{(n)}))| \le \epsilon$ meets a predetermined threshold $\epsilon > 0$. In Section VI, we observe that the proposed scheme can quickly converge to the approximate global optimal solution. Its convergence and monotonicity can be seen in Fig. 6.

V. RADAR-AIDED PC-BASED HYBRID PRECODING SCHEME

In this section, a novel hybrid precoding scheme is presented, as shown in Fig. 4. Specifically, with the aid of radar systems, we consider a hybrid precoding design for the UAV–UGV cooperative system in a more practical scenario, where the FC structure design used in Section III will no longer be appropriate. For this reason, instead of the infinite precision PS with FC structure design, we use a hybrid precoding design with finite precision PS and PC structures.

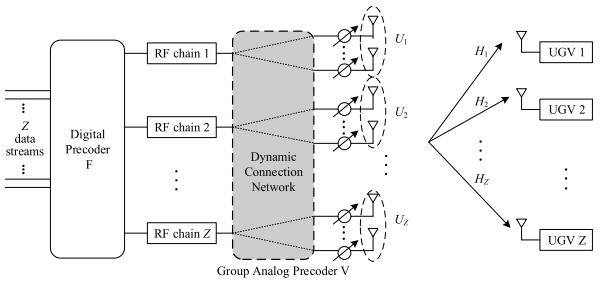

FIGURE 4. Proposed hybrid precoding scheme.

A. PROPOSED DYNAMICALLY CONNECTED HYBRID PRECODING SCHEME

In this part, we address the issue of designing hybrid digital/analog precodes for the PC-HP structure in Fig. 4. Specifically, all transmitting antennas are grouped according to **Algorithm 1** proposed in this section. Then, each RF chain is dynamically connected to disjoined antenna groups through a dynamic connection network. Thus, each entry of the analog precoder $\boldsymbol{V}$ is designed as $v_{i,j} \in \left\{ 0, \frac{1}{\sqrt{N_t}} e^{-j\frac{2\pi n}{2^B}} \middle| n = 0, 1, \ldots, 2^B - 1 \right\}$. Meanwhile, the analog precoder includes only one nonzero element in each row to ensure that distinct subarrays do not overlap, i.e., $\|V(i,:)\|_0 = 1, i = 1, \ldots, N_t$. In particular, it is noted that unlike the weighting sum-rate maximization problems considered in the previous section, this section assumes uniform power allocation, focusing on the process of designing the hybrid digital/analog precoder and no longer considering the power allocation problem. Thus, Equation (9) is

Algorithm 1 Heuristic Algorithm for Hybrid Precoder Design Based on Dynamic Antenna Grouping

Input:

H: channel matrix

B: quantization resolution of phase shifter

$\hat{\theta}_z$: the optimal estimated angle of the z-th UGV, $z = 1, \ldots, Z$

Output:

V: analog precoder

F: digital precoder

1: Initialization:$V = \mathbf{0}$ and U_z=$\emptyset$ for z=1, 2, ..., Z
2: **for** $t = 1, 2 \ldots, N_t$ **do**
3: $z_0 = \arg\max_{1 \le z \le Z} |H_{z,t}|$
4: $U_{z_0} = U_{z_0} \cup \{t\}$
5: **end for**
6: **for** $l = 1, 2, \ldots, Z$ **do**
7: **if** $|U_l| = 0$ **then**
8: $\{t_0, l_{0'}\} = \arg\min_{1 \le l' \le Z, l' \ne l; t \in U_{l'}, U_{l'} \setminus t \ne \emptyset} |H_{l',t}|$
9: $U_{lo'} = U_{lo'} \setminus t_0$
10: $A_l = \{t_0\}$
11: **end if**
12: **end for**
13: **for** $z = 1, 2, \ldots, Z$ **do**
14: **for** $t = 1, 2, \ldots, N_t$ **do**
15: **if** $t \in U_z$ **then**
16: $n_0 = \arg\min_{n \in \{0,1,\ldots,2^B-1\}} \left|\hat{\theta}_z - \frac{2\pi n}{2^B}\right|$
17: $v_{z,t} = e^{j\frac{2\pi n_0}{2^B}}$
18: **end if**
19: **end for**
20: **end for**
21: calculate F according to (42)

re-expressed as

$$SINR_z = \frac{\frac{P}{Z}|\boldsymbol{g}_z^H \boldsymbol{f}_z|^2}{\frac{P}{Z}\sum_{i=1, i\ne z}^{Z} |\boldsymbol{g}_z^H \boldsymbol{f}_i|^2 + \sigma_{n,z}^2} \tag{52}$$

The problem of designing hybrid digital/analog precodes with B bits quantized PSs for the PC-HBF Structure is designed as

$$\{\boldsymbol{V}^{opt}, \boldsymbol{F}^{opt}\} = \arg\max_{\boldsymbol{V},\boldsymbol{F}} \sum_{z=1}^{Z} R_z \tag{53}$$

By analyzing Equation (53), we find that the sum-rate maximization problem corresponds to maximizing the SINR of each UGV. Whereas, directly maximizing SINR per UGV needs the joint design of digital and analog precoders, which is not feasible due to the high computational complexity. Inspired by the findings in [31], [32], in which a two-stage dynamically connected (DC) hybrid precoding scheme was used to solve the above optimization problem, we use the angle parameters obtained by the radar system to directly design the analog precoder, which further reduces the complexity of this PC hybrid precoding scheme. Specifically, first, the transmitting antennas are dynamically grouped, and then the analog precoder is designed in combination with the angle parameters obtained by the radar system to directly maximize $|\boldsymbol{H}_z \boldsymbol{v}_z|$ without considering the inter-UGV interferences. Secondly, in order to eliminate interference between different UGVs, the digital precoding matrix is created using the effective channel matrix.

The digital precoding matrix is calculated according to the effective channel to eliminate the interference between different UGVs.

B. ANTENNA DYNAMIC GROUPING ALGORITHM

According to the above analysis, first, the hybrid precoder design problem in Equation (53) is equivalent to $\max \sum_{z=1}^{Z} |\boldsymbol{H}_z \boldsymbol{v}_z|$. However, maximizing $\sum_{z=1}^{Z} |\boldsymbol{H}_z \boldsymbol{v}_z|$ is in turn equivalent to maximizing each term in the summation. Thus, the optimization problem we need to solve can be formulated as

$$\arg\max_{U_z, \boldsymbol{v}_z} |H_z \boldsymbol{v}_z| \tag{54}$$

$$\text{subject to} \quad C_1 : \sum_{i=1}^{N_t} |\boldsymbol{v}_{z,i}| = |U_z| \ne 0; \quad C_2 : \sum_{z=1}^{Z} |\boldsymbol{v}_{z,i}| = 1. \tag{55}$$

where U_z refers to the group of transmitting antennas linked to the z-th RF chain. $|U_z|$ represents the cardinality of the set U_z. C_1 ensures that the antenna in U_z is exclusively linked to the z-th RF chain, and the RF chain resources will not be wasted because $|U_z| \ne 0$. C_2 guarantees that each antenna is linked with at least one RF chain. In addition, it is necessary to additionally satisfy the condition $U_z \cap U_{z'} \ne \emptyset$, for $z \ne z'$, to ensure that each antenna element is linked to only one RF chain. Finally, the proposed **Algorithm 1** can solve the above optimization problem, as shown above.

In summary, the hybrid precoding algorithm based on a dynamic antenna grouping (DAG) starts by grouping the antennas. It then appends Steps 5 to 12 to ensure user fairness while not wasting RF resources. It is worth pointing out that Steps 2 to 12 are a heuristic method, but its complexity is very low. Steps 13 to 20 use the angle parameters obtained through the radar system to directly design the quantized analog precoding matrix $\boldsymbol{V}$, and the method of acquisition of the angle parameters is described in Section IV. Finally, step 21 designs the digital precoding matrix $\boldsymbol{F}$ by using the BZF algorithm.

VI. SIMULATION RESULTS

This section shows several numerical results obtained through computer simulations to verify the performance of the novel radar-aided location-based hybrid precoding schemes. From Fig. 5 to Fig. 7, we presumed that the UAV-BS was equipped with a ULA of 64 transmit antennas (i.e., $N_t = 64$). In the simulation of the last three pictures, we considered

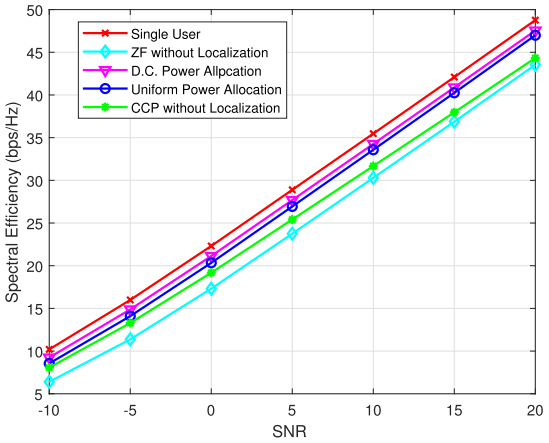

FIGURE 5. Performance comparison for different algorithms (FC-Structures, total transmit antennas $N_t = 64$, and number of UGVs Z = 4).

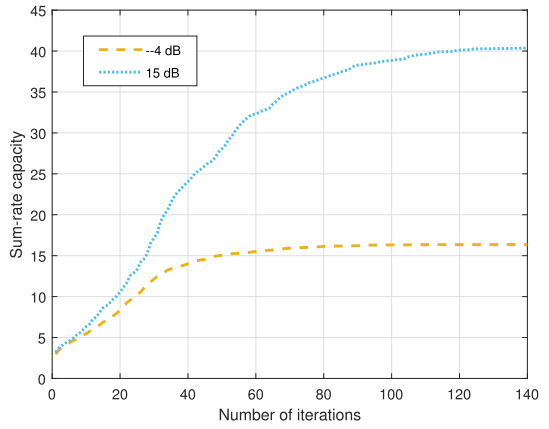

FIGURE 6. Convergence of the proposed D.C. power allocation scheme (with $Z = 4$ UGVs).

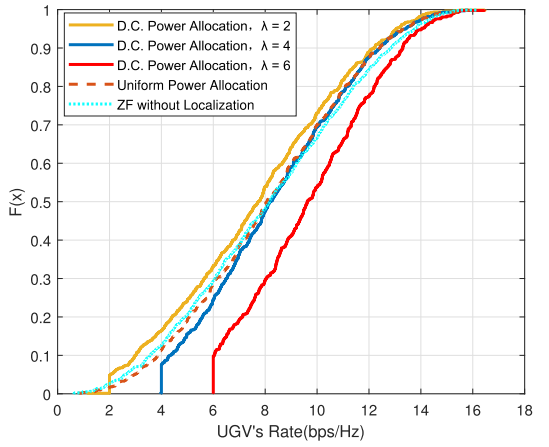

FIGURE 7. The CDF comparison of the UGV's rate with different schemes (total transmit antennas $N_t = 64$, number of UGVs Z = 4).

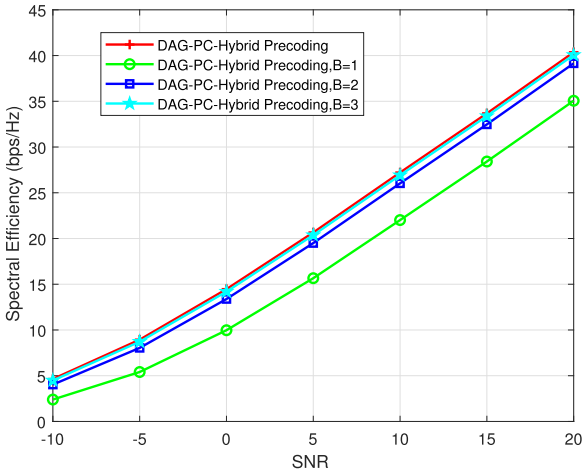

FIGURE 8. The performance of the proposed algorithms with different quantification precision (total transmit antennas $N_t = 128$, number of UGVs Z = 4).

a UAV-BS equipped with a ULA of 128 transmit antennas (i.e., $N_t = 128$). In both cases, the amount of UGVs was four (i.e., Z = 4), and each was equipped with a single-antenna.The total transmit power is constrained by $P = 10$ mW and the initial point $\boldsymbol{\mu}^{(0)}$ is set to $[0.25, 0.25, 0.25, 0.25]$ mW. The amount of propagation paths was given as $L_z = 10$, and $\sigma_z^2 = -10$ dBm for each UGV. The AoDs were uniformly distributed over $[0, 2\pi]$. We calculated the average value of over 100 times for each computer experiment.

In Fig. 5, the spectral efficiency of the conventional hybrid precoding schemes and the proposed radar-aided hybrid precoding scheme are compared. The line "Single User" corresponds to the algorithm proposed in [11] represents a UAV communicating with a UGV. Therefore, the user interference can be completely ignored. The radar-aided hybrid precoding scheme as reported in [34] with uniform power distribution is represented by the "Uniform Power Allocation" curve. The curves labeled "Uniform Power Allocation" and "D.C. Power Allocation" were found to perform similarly where the line labeled "D.C. Power Allocation" represents the algorithm proposed in this paper. The sum-rate, on the other hand, was significantly reduced when location information was not used, as shown on the "ZF without Localization" curve corresponds to the schemes reported in [12]. The cause of this is that the UAV can't accurately distribute the beam to the UGVs. Eventually, the algorithm corresponding to a line labeled "CCP without Localization" is the one reported in [35].

Fig. 6 depicts the proposed D.C. power allocation scheme's convergence behavior under two SNR values of -4 dB and 15 dB, respectively. Fig. 6 reveals the monotonicity and convergence of the proposed scheme under two SNR values.

Next, we verify the QoS for each UGV by setting $\lambda = 2$ bps/Hz, $\lambda = 4$ bps/Hz and $\lambda = 6$ bps/Hz, respectively. Inspection of Fig. 7 shows the CDF of the UGV's rate and the proposed "D.C. Power Allocation" scheme can meet the minimum QoS for each UGV at each set threshold (i.e., 2, 4, 6 bps/Hz). By comparison, when setting $\lambda = 4$ bps/Hz, approximately 10% and 12% of UGVs cannot meet the QoS

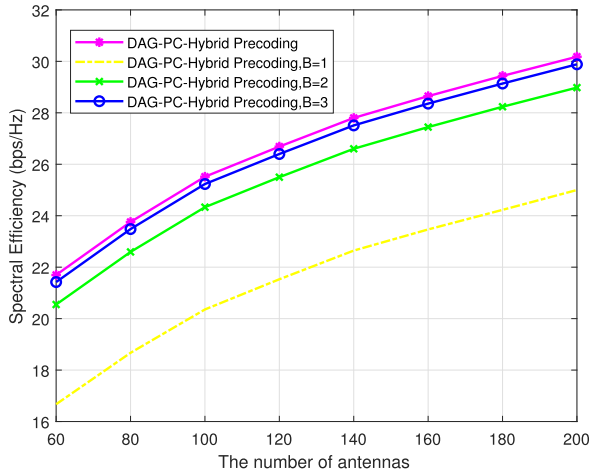

FIGURE 9. Spectyal efficiency versus the number of antennas (number of UGVs Z = 4, SNR = 10 dB).

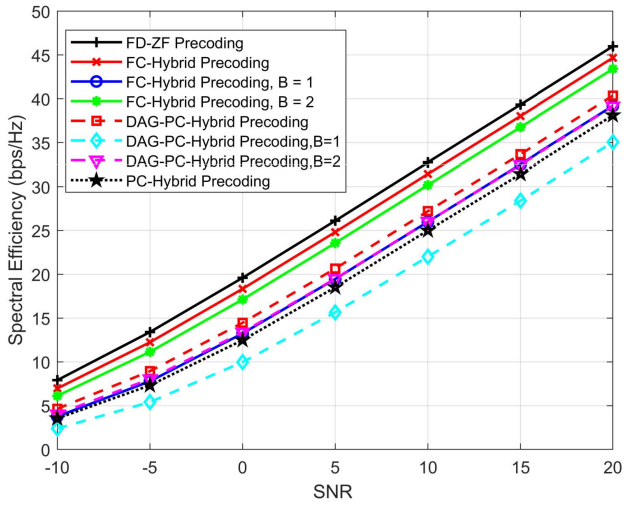

FIGURE 10. Spectral efficiency achieved by different precoding schemes (total transmit antennas $N_t = 128$, number of UGVs Z = 4).

required through the ''uniform power allocation'' scheme and ''ZF without Localization'' scheme.

Fig. 8 depicts the spectral efficiency versus SNR present in the proposed PC-hybrid precoding scheme based on the dynamic antenna grouping (DAG-PC-hybrid precoding) in different quantized phase controls. From Fig. 8, we notice that with the improvement of PS resolution, the behavior of the DAG-PC-hybrid precoding scheme is better.

Fig. 9 depicts the spectral efficiency versus the amount of antennas of proposed radar-aided PC-based hybrid precoding schemes. Under the given situation, we set the number of user to $Z = 4$ and SNR = 10 dB. From Fig. 9, we can also expect that with the growth of number of antennas N_t, the behavior of sum-rate will be enhanced by providing more diversity and precoding gain.

Fig. 10 depicts the spectral efficiency versus SNR of the proposed radar-aided hybrid precoding schemes, in which the PS is quantized to 1 bit and 2 bit, respectively. In order to compare the schemes better, we also added two schemes: a traditional fully-digital-zero-forcing (FD-ZF) precoding scheme [12] and a traditional PC-hybrid precoding scheme [33]. It can be observed from Fig. 10 that the DAG-PC-hybrid precoding scheme always has better behavior than the PC-hybrid precoding scheme. Specifically, the curve ''FC-hybrid precoding, B = 1'' and ''DAG-PA-hybrid precoding, B = 2'' have comparable performance.

VII. CONCLUSION

In our work, we developed two novel location-based hybrid precoding schemes for a radar-aided UAV–UGV heterogeneous cooperative system. On the basis of radar-assisted communications, we decomposed the hybrid precoders design problem into two sub-problems, namely localization and communication. First, the specific location of the UGV was detected by the radar loaded on the UAV. Then, using the location information obtained from the UGVs, location-based precoding was accomplished. Next, two radar-aided hybrid precoding schemes were designed. In the first scheme, with the assistance of the radar system, the joint design of hybrid precoding and power allocation was proposed to maximize the sum-rate based on D.C. programming. The latter scheme mainly considered more practical scenes. Using phase shifters with limited precision, a heuristic algorithm based on antenna dynamic grouping was designed to maximize the sum-rate. Finally, we used a computer simulation to validate the efficacy of our proposed novel location-based hybrid precoding schemes for the radar-aided UAV–UGV cooperative systems.

ACKNOWLEDGMENT

An earlier version of this paper was presented in part at the International Conference on Wireless Communications and Signal Processing (WCSP), Changsha, China, October 2021 [1].

REFERENCES

[1] X. Xu, Y. Qian, R. Zhang, and X. Yang, ''Integrated radar-aided localization and QoS-aware communications for UAV-UGV cooperative systems,'' in *Proc. 13th Int. Conf. Wireless Commun. Signal Process. (WCSP)*, Changsha, China, Oct. 2021, pp. 1–6.

[2] Y. Wu, S. Wu, and X. Hu, ''Cooperative path planning of UAVs & UGVs for a persistent surveillance task in urban environments,'' *IEEE Internet Things J.*, vol. 8, no. 6, pp. 4906–4919, Mar. 2021.

[3] Z. Kashino, G. Nejat, and B. Benhabib, ''Aerial wilderness search and rescue with ground support,'' *J. Intell. Robotic Syst.*, vol. 99, no. 1, pp. 147–163, Nov. 2019.

[4] J. Li, G. Deng, C. Luo, Q. Lin, Q. Yan, and Z. Ming, ''A hybrid path planning method in unmanned air/ground vehicle (UAV/UGV) cooperative systems,'' *IEEE Trans. Veh. Technol.*, vol. 65, no. 12, pp. 9585–9596, Dec. 2016.

[5] M. Xiao, S. Mumtaz, Y. Huang, L. Dai, Y. Li, M. Matthaiou, and G. K. Karagiannidis, ''Millimeter wave communications for future mobile networks,'' *IEEE J. Sel. Areas Commun.*, vol. 35, no. 9, pp. 1909–1935, Sep. 2017.

[6] T. S. Rappaport, S. Sun, R. Mayzus, H. Zhao, Y. Azar, K. Wang, G. N. Wong, J. K. Schulz, M. Samimi, and F. Gutierrez, ''Millimeter wave mobile communications for 5G cellular: It will work!'' *IEEE Access*, vol. 1, pp. 335–349, 2013.

[7] A. F. Molisch, V. V. Ratnam, S. Han, Z. Li, S. Le Hong Nguyen, L. Li, and K. Haneda, "Hybrid beamforming for massive MIMO: A survey," *IEEE Commun. Mag.*, vol. 55, no. 9, pp. 134–141, Sep. 2017.

[8] R. W. Heath, Jr., N. González-Prelcic, S. Rangan, W. Roh, and A. M. Sayeed, "An overview of signal processing techniques for millimeter wave MIMO systems," *IEEE J. Sel. Topics Signal Process.*, vol. 10, no. 3, pp. 436–453, Apr. 2016.

[9] C. H. Doan, S. Emami, D. A. Sobel, A. M. Niknejad, and R. W. Brodersen, "Design considerations for 60 GHz CMOS radios," *IEEE Commun. Mag.*, vol. 42, no. 12, pp. 132–140, Dec. 2004.

[10] F. Sohrabi and W. Yu, "Hybrid digital and analog beamforming design for large-scale antenna arrays," *IEEE J. Sel. Topics Signal Process.*, vol. 10, no. 3, pp. 501–513, Apr. 2016.

[11] O. El Ayach, S. Rajagopal, S. Abu-Surra, Z. Pi, and R. W. Heath, Jr., "Spatially sparse precoding in millimeter wave MIMO systems," *IEEE Trans. Wireless Commun.*, vol. 13, no. 3, pp. 1499–1513, Mar. 2014.

[12] L. Liang, W. Xu, and X. Dong, "Low-complexity hybrid precoding in massive multiuser MIMO systems," *IEEE Wireless Commun. Lett.*, vol. 3, no. 6, pp. 653–656, Dec. 2014.

[13] X. Gao, L. Dai, S. Han, I. Chih-Lin, and R. W. Heath, Jr., "Energy-efficient hybrid analog and digital precoding for mmWave MIMO systems with large antenna arrays," *IEEE J. Sel. Areas Commun.*, vol. 34, no. 4, pp. 998–1009, Apr. 2016.

[14] X. Yu, J. Shen, J. Zhang, and K. B. Letaief, "Alternating minimization algorithms for hybrid precoding in millimeter wave MIMO systems," *IEEE J. Sel. Topics Signal Process.*, vol. 10, no. 3, pp. 485–500, Feb. 2016.

[15] J.-C. Chen, "Hybrid beamforming with discrete phase shifters for millimeter-wave massive MIMO systems," *IEEE Trans. Veh. Technol.*, vol. 66, no. 8, pp. 7604–7608, Aug. 2017.

[16] J. Zhang, Y. Huang, J. Wang, and L. Yang, "Hybrid precoding for wideband millimeter-wave systems with finite resolution phase shifters," *IEEE Trans. Veh. Technol.*, vol. 67, no. 11, pp. 11285–11290, Nov. 2018.

[17] X. Gao, L. Dai, Y. Sun, S. Han, and I. Chih-Lin, "Machine learning inspired energy-efficient hybrid precoding for mmWave massive MIMO systems," in *Proc. IEEE Int. Conf. Commun.*, Paris, France, May 2017, pp. 1–6.

[18] Z. Pi and F. Khan, "An introduction to millimeter-wave mobile broadband systems," *IEEE Commun. Mag.*, vol. 49, no. 6, pp. 101–107, Jun. 2011.

[19] L. Zhu, J. Zhang, Z. Xiao, X. Cao, X.-G. Xia, and R. Schober, "Millimeter-wave full-duplex UAV relay: Joint positioning, beamforming, and power control," *IEEE J. Sel. Areas Commun.*, vol. 38, no. 9, pp. 2057–2073, Sep. 2020.

[20] J. A. Zhang, M. L. Rahman, K. Wu, X. Huang, Y. J. Guo, S. Chen, and J. Yuan, "Enabling joint communication and radar sensing in mobile networks—A survey," *IEEE Commun. Surveys Tuts.*, vol. 24, no. 1, pp. 306–345, Oct. 2022.

[21] F. Liu, C. Masouros, A. P. Petropulu, H. Griffiths, and L. Hanzo, "Joint radar and communication design: Applications, state-of-the-art, and the road ahead," *IEEE Trans. Commun.*, vol. 68, no. 6, pp. 3834–3862, Jun. 2020.

[22] A. Al-Hourani, S. Kandeepan, and S. Lardner, "Optimal LAP altitude for maximum coverage," *IEEE Wireless Commun. Lett.*, vol. 3, no. 6, pp. 569–572, Dec. 2014.

[23] S. Shaham, M. Ding, M. Kokshoorn, Z. Lin, S. Dang, and R. Abbas, "Fast channel estimation and beam tracking for millimeter wave vehicular communications," *IEEE Access*, vol. 7, pp. 141104–141118, 2019.

[24] J. Li and P. Stoica, *MIMO Radar Signal Processing*. Hoboken, NJ, USA: Wiley, 2008.

[25] S. Sand, A. Dammann, and C. Mensing, *Positioning in Wireless Communications Systems*. Hoboken, NJ, USA: Wiley, 2014.

[26] W. Yuan, Z. Wei, S. Li, J. Yuan, and D. W. K. Ng, "Integrated sensing and communication-assisted orthogonal time frequency space transmission for vehicular networks," *IEEE J. Sel. Topics Signal Process.*, vol. 15, no. 6, pp. 1515–1528, Nov. 2021.

[27] F. Liu, W. Yuan, C. Masouros, and J. Yuan, "Radar-assisted predictive beamforming for vehicular links: Communication served by sensing," *IEEE Trans. Wireless Commun.*, vol. 19, no. 11, pp. 7704–7719, Nov. 2020.

[28] T. Jia, K. C. Ho, H. Wang, and X. Shen, "Localization of a moving object with sensors in motion by time delays and Doppler shifts," *IEEE Trans. Signal Process.*, vol. 68, pp. 5824–5841, 2020.

[29] H. H. Kha, H. D. Tuan, and H. H. Nguyen, "Fast global optimal power allocation in wireless networks by local D.C. Programming," *IEEE Trans. Wireless Commun.*, vol. 11, no. 2, pp. 510–515, Feb. 2012.

[30] H. Tuy, *Convex Analysis and Global Optimization*. Dordrecht, The Netherlands: Academic, 1998.

[31] X. Zhu, Z. Wang, L. Dai, and Q. Wang, "Adaptive hybrid precoding for multiuser massive MIMO," *IEEE Commun. Lett.*, vol. 20, no. 4, pp. 776–779, Apr. 2016.

[32] X. Jing, L. Li, H. Liu, and S. Li, "Dynamically connected hybrid precoding scheme for millimeter-wave massive MIMO systems," *IEEE Commun. Lett.*, vol. 22, no. 12, pp. 2583–2586, Dec. 2018.

[33] S. Han, I. Chih-Lin, Z. Xu, and C. Rowell, "Large-scale antenna systems with hybrid analog and digital beamforming for millimeter wave 5G,' *IEEE Commun. Mag.*, vol. 53, no. 1, pp. 186–194, Jan. 2015.

[34] A. Alkhateeb, G. Leus, and R. W. Heath, Jr., "Limited feedback hybrid precoding for multi-user millimeter wave systems," *IEEE Trans. Wireless Commun.*, vol. 14, no. 11, pp. 6481–6494, Nov. 2015.

[35] B. Hu, C. Hua, C. Chen, and X. Guan, "Joint beamformer design for wireless fronthaul and access links in C-RANs," *IEEE Trans. Wireless Commun.*, vol. 17, no. 5, pp. 2869–2881, May 2018.

XIANGQIAN XU (Student Member, IEEE) received the B.S. degree in electronic and information engineering from Hunan Institute of Engineering, Xiangtan, China, in 2018. He is currently pursuing the master's degree in electronic information with Jishou University. His research interests include hybrid precoding, array signal processing, and MIMO communications.

RENMIN ZHANG (Member, IEEE) received the B.S. degree in electrical engineering from the Guilin University of Electronic Technology, Guilin, China, in 2003, the M.S. degree in electronic and communication engineering from Peking University, Beijing, China, in 2011, and the Ph.D. degree in information and communication engineering form Southeast University, Nanjing, China, in 2019. Since 2019, he has been an Associate Professor with the School of Information Science and Engineering of Jishou University. His research interests include MIMO communications, signal processing, and THz communications.

YINGJING QIAN received the B.S. degree in communications engineering from Nanchang University, Nanchang, China, in 2004, and the M.S. degree in circuits and systems from Hunan University, Changsha, China, in 2011. She is currently an Associate Professor with the College of Electrical and Information Engineering, Huaihua University. Her research interests include wireless communications and machine learning.